

Neutron Background Signal in Superheated Droplet Detectors of the Phase II SIMPLE Dark Matter Search

A.C. Fernandes^{1,†}, A. Kling¹, M. Felizardo², T.A. Girard², A.R. Ramos¹,
J.G. Marques¹, M.I. Prudêncio¹, R. Marques¹, F.P. Carvalho¹, I. Lázaro³
(for the SIMPLE Collaboration)

¹ Centro de Ciências e Tecnologias Nucleares (C2TN), Instituto Superior Técnico, Universidade de Lisboa.
Estrada Nacional 10 (km 139.7), 2695-066 Bobadela LRS, Portugal

² Departamento de Física, Faculdade de Ciências, Universidade de Lisboa. Campo Grande, Building C8,
1749-016 Lisboa, Portugal

³ Laboratoire Souterrain à Bas Bruit, University of Nice, University of Avignon, Centre National de la Recherche
Scientifique, Aix-Marseille University, Observatoire de la Côte d'Azur, 84400 Rustrel, France

[†] corresponding author: anafer@ctn.ist.utl.pt

Key words: dark matter; superheated liquids; background; simulation

Abstract

The simulation of the neutron background for Phase II of the SIMPLE direct dark matter search experiment is described, including further improvements relatively to previously reported data. Spontaneous fission and decay-induced (α,n) reactions originating in ^{238}U and ^{232}Th naturally present in the experiment materials were considered. The model employs the Monte Carlo MCNP neutron transport code, using a realistic geometry description and measured radioassays and material compositions as input. Tabled (α,n) yields, measured detection efficiencies and evaluated cross section data were used. The energy distribution of the recoiling nuclei is dealt with a distinct code. A thorough uncertainty analysis of the simulated results is performed that addresses statistical and most non-statistical uncertainties. The estimated recoil event rate is $0.367 \pm 0.002(\text{stat.}) \pm 0.064$ (non-stat.) evt/kgd, a 10% increase in the previous reported result.

1. Introduction

Direct dark matter search experiments are based on the observation of nuclear recoils induced by the elastic scattering of Weakly Interacting Massive Particles (WIMPs) with target nuclei. SIMPLE (Superheated Instrument for Massive Particle Search) is one of three international

experiments using superheated liquids: SIMPLE and PICASSO have employed superheated droplet detectors (SDDs) while COUPP uses bubble chambers for increased active mass and has recently merged with PICASSO into PICO [1-4].

An SDD is a suspension of micrometric superheated liquid droplets in a viscoelastic gel which undergo transitions to the gas phase upon absorption of energy from radiation [5]. A proto-bubble will expand to a millimeter-sized bubble when two thermodynamically-defined threshold conditions are verified with respect to (i) the energy deposited and (ii) the distance within the droplet where the deposition occurs [6]. SIMPLE employs C_2ClF_5 in a food gel-based matrix and operates at $9^\circ C$ and 2 bar. A critical energy deposition $E_{crit}=8.2$ keV and Linear Energy Transfer $LET_{crit}=159.7$ keV μm^{-1} are required for a bubble nucleation, which is detected via an acoustic instrumentation and signal analysis that confer and identify its characteristic frequency signature [7].

Expected WIMP-nucleon interaction rates are extremely small, below 10^{-3} event (evt) per kilogram of detector mass and day (kgd). The key to the direct search experiments lies in the ability to suppress and reject more prevalent signals originating in cosmic radiation and natural radioactivity. Background reduction is generally achieved through operation in underground facilities, additional radiation shielding, purification of detector components and radon purging. As the threshold conditions render SIMPLE SDDs intrinsically insensitive to low linear energy transfer radiations (e.g. photons and electrons), the detector background signal is restricted to alpha particles and neutrons, which are discriminated based on signal amplitude [8,9].

The reduction and assessment of the neutron background are crucial because fast neutrons interact with nuclei through elastic scattering, mimicking the characteristic signal expected from WIMPs. In deep underground facilities neutrons originate primarily from emitters present at trace levels in the facility and detector materials. Among the naturally occurring emitters ^{238}U and ^{232}Th are the most important, producing neutrons both by spontaneous fission (with low branching ratios) and (α,n) reactions – alphas being emitted by the various descendants in the decay series. Neutron energies up to 10-20 MeV are involved, which are sufficiently high to travel cross significant shielding thicknesses.

In direct dark matter search, the reduced neutron field intensity hampers the experimental determination of the neutron background due to, e.g., insufficient sensitivity, electronic noise or dose during transport. Simulation techniques have a leading role in the determination of the neutron background, namely through the application of general-purpose Monte Carlo (MC) neutron transport simulation codes. MCNP, GEANT and FLUKA [10-12] have been used by most experiments to optimize the neutron shielding, simulate detector responses, interpret the detector signal, select the experiment materials, and estimate or calculate the neutron-induced detector background signal [13-24]. The application of FLUKA is restricted to the muon-induced neutrons, while GEANT offers the possibility to calculate both the muon-induced and the “local” neutron component, and can be applied to a broad scope of interactions – which contributed to its wide acceptance. In general (α ,n) reaction yields and spectra were extracted by the SOURCES-4C code [25]; in some cases the code limitations were overcome by in-house developments. With respect to MCNP-based codes, we note the application of MCNP by CRESST, and of MCNP-PoliMi [26] by COUPP for detector background calculations normalized to the results of material radio-assays. In order to obtain the recoil spectra the evaluation of a raw data output file of MCNP is facilitated within MCNP-PoliMi.

The present paper reports the calculations for the latest SIMPLE experiment using MCNP and alternative approaches to derive the (α ,n) data sources and recoil spectra. The current results include various developments relatively to the findings previously reported [1,27]. The additional studies include the evaluation of events induced by nuclear reactions not considered so far, contributions due to materials omitted in previous studies, influence of the energy distribution of the recoils and a significant improvement of the uncertainty evaluation.

2. Experimental Set-up

SIMPLE was run in the GESA facility of Laboratoire Souterrain à Bas Bruit (LSBB, southern France) [28]. GESA is a 60 m³ room at a depth of 500 m within LSBB, corresponding to 1500 m water-equivalent (mwe) depth. Floor plan dimensions are (400 x 564) cm². The ceiling has a semi-cylindrical shape (diameter 404 cm), the room height varying between 212 and 305 cm. The surrounding rock is calcite. Room walls, ceiling and floor consist of concrete, with a thickness between 30 and 100 cm. The room is equipped with a 1 cm-thick steel lining forming a Faraday cage that shields against electromagnetic noise.

Each SDD consisted of a 900 ml glycerine-based gel matrix with a 1-2 wt.% suspension of C_2ClF_5 . The detector container was a (9 x 9 x 12) cm^3 flask of laboratory borosilicate glass (BSG), with a thickness of 5 mm. A 2 cm glycerine layer above the gel embeds the microphone employed in the acoustic instrumentation and reduced the diffusion of atmospheric radon.

The experiment used fifteen SDDs installed in a water bath with a cross-sectional dimension of (97 x 130) cm^2 , in the central region of the room. The SDDs were distributed in alternating positions in a 16 cm square lattice. A water layer of 3 cm above the glycerine level further reduced radon diffusion and improved the thermal equilibrium in the detector.

GESA's room floor contains several steel-covered, 50 cm deep crawl spaces previously used for cable conduits. Some of them are located around the tank, which is supported by a concrete pedestal. The tank walls consisted of glass-reinforced plastic (GRP) with a thickness of 5mm and was surrounded by 5 cm of polyurethane foam for acoustic insulation.

A preliminary evaluation of the original SIMPLE set-up in GESA (Phase I, 2004-2007) [29] demonstrated the need to implement a neutron shield for reducing the neutron-induced event rate well below 1 evt/kgd [30]. Phase II of SIMPLE (2009-2011) comprised two stages of measurements [8,27] performed under a shielded configuration using water as neutron moderator. The neutron shielding consisted of a pile of 20 liter water boxes (22 x 25 x 38) cm^3 , symmetrically installed around and above the tank to produce water thicknesses of 50-75 cm, respectively. The SDDs were raised 50 cm above the tank floor for additional shielding from neutrons emitted by the pedestal. The pedestal is surrounded by water boxes, producing a shield of 44 cm width and 50 cm height.

Stage 1 (2009-2010) was carried out with a net exposure of 11.53 kgd achieving a measured event rate of 0.61 evts/kgd. The calculation of the neutron background suggested that a relevant improvement in the shielding would be gained using additional hydrogen-based shielding. With the purpose to reduce the neutron contribution from the pedestal, the tank (originally sitting on a wooden support structure with 18 cm thickness) was raised above the concrete floor in order to accommodate a polyethylene block of 10 cm thickness and a wooden layer (2 cm) between the tank and the wooden support. The free spaces underneath the wooden platform were filled with additional polyethylene (10 cm thickness), paraffin (8

cm) and wood (4 cm). Finally, as the water boxes become slightly deformed due to the weight loading, direct channels across the lateral shielding were eliminated with an overlapping box arrangement. The last stage of measurements (Stage 2, 2010-2011) involved an exposure of 6.71 kgd and 0.15 evts/kgd.

Figure 1 presents the geometrical model employed in the simulations of the SIMPLE set-up in GESA. Some structures were removed from the figure for clarity (rock, concrete and steel in the front and right walls, water boxes in the front and right side of the tank and the tank water surrounding the detectors). Surrounding the cavern, uniform layers of concrete and rock were considered with thicknesses of 30 cm and 1 m respectively, after evaluating the effect of these parameters on the calculated background [30].

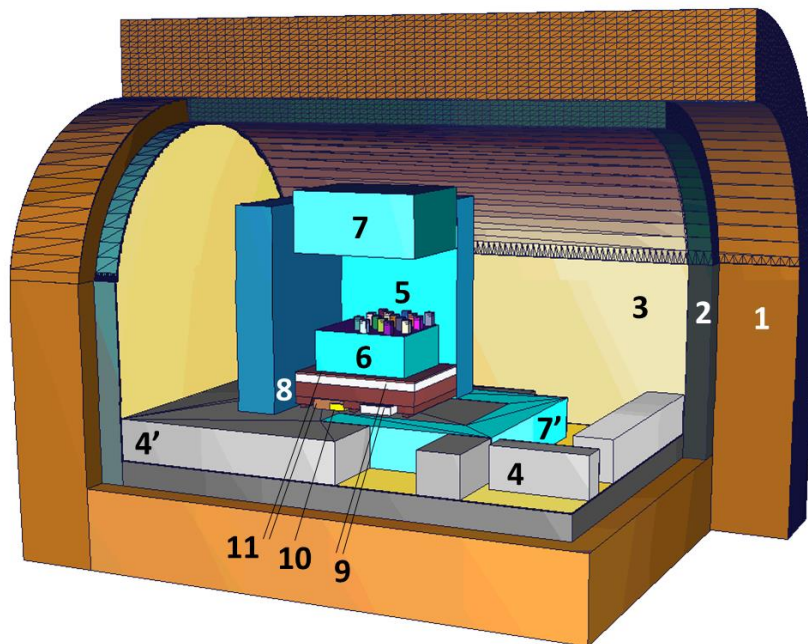


Fig. 1: Geometry model for the MCNP calculations of the neutron background in the final stage of SIMPLE Phase II.

- 1: rock; 2: concrete walls, floor and ceiling; 3: steel lining; 4: concrete floor structures defining cable conduits; 4': tank pedestal; 5: detectors; 6: tank (water below the detectors);
- 7: water shield around and above the tank; 7': water shield around the tank pedestal;
- 8: wood support; 9: polyethylene shield (layer and insert); 10: paraffin insert;
- 11: wood layer and insert.

3. Simulation Strategy

Version 4C of MCNP was used in the simulations. Transport cross sections were taken mostly from the ENDF-B6.0 library included in the package.

Fluence rates were calculated using the track-length estimator of MCNP (F4 tally) in the active volume of the detectors. MCNP yields group fluence rates, i.e. fluence rates of neutrons with energies within the limits of a user-defined bin structure. Our group structure consisted of equi-lethargy groups in number of three per decade between 0.1 meV and 1 keV, and ten per decade from 1 keV to 20 MeV.

The calculation of reaction rates was separated from the MCNP simulations in order to facilitate the evaluation of aspects related to reaction cross section data. The FLXPRO code of the LSL-M2 package [31] was employed to determine the average cross sections corresponding to our group structure. Reaction cross sections and variances were obtained from the ENDF-B7.1 library [32].

MCNP outputs are given relative to one source neutron, and must be scaled to the actual source emission rate in order to obtain absolute results. Besides its emission rate, the source is characterized in terms of location, energy and angular distribution of the emitted neutrons. Theoretical (analytical or tabled) distributions are used to describe the energy spectrum of the source neutrons. The contributions of ^{238}U and ^{232}Th in each material were considered individually, assuming uniform emitter distribution and isotropic emission. The various source materials and reactions were also discriminated in order to evaluate their relative contribution to the overall event rate.

Most data on event rate herein reported were calculated assuming maximum energy transfer, i.e. the case of a head-on collision, from the neutron to the recoiling nucleus. This overestimates the event rate, since the scattering reaction has an angular distribution and the recoil energy decreases with decreasing scattering angle. This effect leaves a fraction of the recoil nuclei with energies below the threshold for event production. The distribution of the recoiling nuclei was considered at a final stage for the total neutron spectrum using the full version of the SPECTER code [33].

4. Material Data

4.1 Composition

Material composition plays an important role in neutron attenuation and production. Light nuclei are the most relevant, since they maximize the neutron energy transfer in elastic collisions, and may exhibit high cross sections for (α,n) reactions. For SIMPLE it was essential to quantify (i) hydrogen in wood allowing to model the moderation of neutrons emitted by the concrete pedestal, and (ii) boron in BSG in order to define the production of (α,n) neutrons in the detector containers.

Ion beam-based techniques are particularly adequate to quantify light elements, and were applied at C2TN, Portugal. Elastic recoil detection using a 2 MeV He^+ beam was applied to determine the ^1H content in wood, the remaining elements being quantified simultaneously by Rutherford Backscattering (RBS). The amount of ^{11}B in glass was measured by Nuclear Reaction Analysis and Resonant Elastic Scattering, while the other elements were determined by RBS in the same run. For optimization of the detection conditions a 1.55 MeV proton beam has been employed for these measurements.

Chemical analyses performed at the University of Avignon, France yielded the mineral composition of rock and concrete.

The composition of the steel GESA lining and the microphone were assumed to be 100% iron. Standard compositions for air (volume composition 78% N_2 + 21% O_2 + 1% Ar), water (H_2O), glycerin ($\text{C}_3\text{H}_8\text{O}_3$), paraffin ($\text{C}_{25}\text{H}_{52}$) and polyethylene (CH_2) were used.

The GRP forming the tank walls was assumed to be the commonly used polypropylene (C_3H_5) reinforced with fibers of E-glass whose density ($2.55\pm 0.03 \text{ g cm}^{-3}$) and composition ranges were obtained from reference data [34]; the average values of the range limits were used in the model. The E-glass (typically 10-30 wt.% in GRP) was not included in the GRP description. A microscope image of the GRP (Fig. 2) confirm that, similarly to other GRPs [35] the individual fibers form a compact roving which can be considered as a unique fiber. The measured diameters of the individual fiber and roving are $20\pm 1 \mu\text{m}$ and $300\pm 20 \mu\text{m}$ respectively.

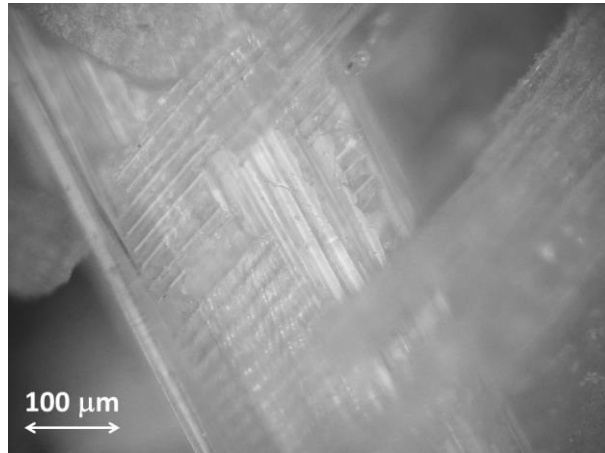


Fig. 2: Glass fibers emerging from the GRP, 200x. Rovings of different orientations are shown, the proximal being partly broken near its edge.

The mass composition of the gel matrix is 1.71% gelatin, 4.18% polyvinylpyrrolidone (C_6H_6NO), 15.48% water and 78.16% glycerin and 0.47% agarose ($C_6H_6O_6$) [36]. In order to derive the elemental composition of the gel matrix, the following mass composition was assumed for gelatin: 12.5% proline ($C_6H_6NO_6$), 12.5% hydroxyproline ($C_6H_6NO_6$), 20% glycine ($C_6H_6NO_6$), 23% glutamic acid ($C_6H_6NO_6$) representing also other non-essential amino acids, 16% arginine ($C_6H_6N_6O_6$) and 16% alanine ($C_6H_6NO_6$), each including half of the other essential amino acids [37].

Standard densities were considered for steel (7.874 g cm^{-3}), air ($1 \times 10^{-3} \text{ g cm}^{-3}$), water (1 g cm^{-3}) and glycerin (1.261 g cm^{-3}). The densities of wood, paraffin ($0.83 \pm 0.01 \text{ g cm}^{-3}$), polyethylene ($0.95 \pm 0.01 \text{ g cm}^{-3}$), bulk microphone ($1.98 \pm 0.01 \text{ g cm}^{-3}$), GRP ($1.05 \pm 0.01 \text{ g cm}^{-3}$), BSG, concrete and rock were measured by the immersion method, their uncertainties reflecting mainly those in the volume measurement. The density of the gel matrix was initially calculated considering the nominal mass (1183 g) and volume (900 cm^3). The final value and its uncertainty are derived from a comparison with the density of the superheated liquid at the thermodynamic operating conditions (1.33 g cm^{-3}), considering that density matching is achieved for detector fabrication.

Table 1 summarizes the results obtained. For BSG and wood a good agreement was found between measured and nominal compositions [38,39]. The nominal data for BSG corresponds to the material used in the experiment.

Table 1: Materials composition and density. In the cases of borosilicate glass (BSG), E-glass and wood, nominal compositions are given in brackets. For E-glass, the range limits for B₂O₃ are detailed.

a) Inorganic materials

| | Rock | Concrete | BSG | E-glass |
|---------------------------------|-----------|-----------|----------------|-------------|
| Composition (wt.%) | | | | |
| SiO ₂ | | 37.20 | 81.8±3.3 (81) | (55) |
| Al ₂ O ₃ | | 3.58 | 2.3±0.09 (2) | (14) |
| Fe ₂ O ₃ | | 1.40 | | (0.3) |
| MnO | | 0.05 | | |
| MgO | 0.31 | 0.75 | | (2.2) |
| CaO | | | | (22) |
| Ca ₂ CO ₃ | 99.69 | 55.42 | | |
| Na ₂ O | | 0.67 | 2.0±0.08 (2) | (0.5) |
| K ₂ O | | 0.72 | 1.5±0.06 (2) | |
| TiO ₂ | | 0.15 | | (0.5) |
| P ₂ O ₅ | | 0.06 | | |
| B ₂ O ₃ | | | 12.4±0.50 (13) | (5 [4-6]) |
| F ₂ | | | | (0.5) |
| Density (g cm ⁻³) | 2.61±0.01 | 2.39±0.01 | 2.23±0.01 | (2.55±0.03) |

b) Organic materials

| | Wood | Gel matrix |
|-------------------------------|-----------|------------|
| Composition (wt. %) | | |
| H | 5.8 (6) | 9.10 |
| C | 47.6 (50) | 33.80 |
| O | 46.0 (44) | 56.35 |
| K | 0.6 (0) | |
| N | | 0.75 |
| Density (g cm ⁻³) | 0.51±0.01 | 1.32±0.01 |

4.2 Radioactive Contaminants

Traces of ^{238}U and ^{232}Th in most experiment materials were quantified via low detection limit techniques. The gel was evaluated in an early phase of SIMPLE by α -spectroscopy at Pacific Northeast National Laboratory, USA. Alpha spectroscopy was also used at C2TN to analyze the wood and shielding water after incineration and evaporation, respectively. The structural materials of GESA (concrete, rock and steel) were assayed by low-background gamma spectroscopy at the Laboratoire Souterrain de Modane, France. The paraffin and polyethylene used in the shielding, the GRP tank walls, the BSG detector container and the microphone were evaluated at C2TN by Neutron Activation Analysis (NAA) using the comparative method, i.e., through co-irradiation with standard materials certified for ^{238}U or ^{232}Th concentration. The evaluation of most materials by NAA employed two standards and three samples, which is particularly suitable for heterogeneous materials like GRP.

Spectroscopic methods can provide information about various radioisotopes of the ^{238}U and ^{232}Th decay chain and thereby allows the evaluation of secular equilibrium. In contrast, NAA can only quantify radionuclides for which certified reference materials are available.

Table 2 shows the measured amounts of ^{238}U and ^{232}Th in the various materials. The experimental uncertainties are reported at the $1-\sigma$ (68% confidence) level. Available information about radioactive descendants naturally produced through the decay series of ^{238}U or ^{232}Th is included. When the measurement is below the detection limit (e.g., paraffin, gel), the latter is given.

The activity concentrations of ^{238}U and ^{232}Th in concrete were measured through the detection of the third generation, short-lived descendants $^{234\text{m}}\text{Pa}$ and ^{238}Ac , respectively. The measurements for steel, water and wood confirm the absence of secular equilibrium in these materials. For steel it was deduced that the activity of ^{232}Th is equal to that of its chemically identical decay isotope ^{228}Th , while ^{238}U activity is equal to that of ^{234}Th – a direct descendent (2^{nd} generation) with a half-life of 24 d, which is much smaller than the steel age (LSBB was built in the late seventies). In the cases of water and wood secular equilibrium was assumed at the measured activities of ^{232}Th and ^{238}U .

Table 2: Activity concentration of ^{238}U and ^{232}Th in GESA and SIMPLE materials (Bq l^{-1} for water and Bq kg^{-1} for other materials).

| Material | Method | ^{238}U | ^{232}Th |
|----------------------|------------------|--|---|
| Concrete | γ -spectr | 10.5 ± 1.0 | 7.7 ± 0.2 |
| Gel | α -spectr | $< 9.0 \times 10^{-3}$ | - |
| BSG | NAA | 2.74 ± 0.41 | 1.27 ± 0.11 |
| Microphone | NAA | < 13.6 | - |
| Paraffin | NAA | < 0.25 | < 0.4 |
| Polyethylene | NAA | $3.99 \times 10^{-1} \pm 1 \times 10^{-3}$ | - |
| Polyurethane | NAA | 0.58 ± 0.15 | < 0.4 |
| Rock | γ -spectr | 5.0 ± 2.5 | $1.6 \times 10^{-1} \pm 1.3 \times 10^{-2}$ |
| Steel ⁽¹⁾ | γ -spectr | $3.6 \times 10^{-2} \pm 1.1 \times 10^{-2}$ | $1.3 \times 10^{-2} \pm 1 \times 10^{-3}$ |
| GRP | NAA | 7.76 ± 0.49 | 18.0 ± 1.9 |
| Water ⁽²⁾ | α -spectr | $3.20 \times 10^{-2} \pm 6.0 \times 10^{-4}$ | $5.00 \times 10^{-5} \pm 1.00 \times 10^{-5}$ |
| Wood ⁽³⁾ | α -spectr | $1.07 \times 10^{-1} \pm 1.5 \times 10^{-2}$ | $3.0 \times 10^{-3} \pm 9.0 \times 10^{-4}$ |

Additional radioisotope activities:

- (1) ^{238}U series: $^{226}\text{Ra}=10 \pm 1 \text{ mBq kg}^{-1}$; $^{210}\text{Pb}=1.74 \pm 0.2 \text{ Bq kg}^{-1}$.
 ^{232}Th series: $^{228}\text{Ra}=6 \pm 2 \text{ mBq kg}^{-1}$
- (2) ^{238}U series : $^{234}\text{U}=121 \pm 17 \text{ mBq kg}^{-1}$; $^{230}\text{Th}=8.6 \pm 1.5 \text{ mBq kg}^{-1}$
- (3) ^{238}U series: $^{234}\text{U}=42.4 \pm 0.8 \text{ mBq l}^{-1}$; $^{230}\text{Th}=7.0 \times 10^{-2} \pm 9 \times 10^{-3} \text{ mBq l}^{-1}$

5. Neutron Source

5.1 Spontaneous Fission

The energy spectrum of neutrons emitted by the spontaneous fission of ^{238}U and ^{232}Th is described by a Watt formula: $e^{-E/a} \sinh(bE)/2$, with a and b being radionuclide-specific fission parameters obtained from the SOURCES-4A data file [40] and E the neutron energy. Neutron multiplicities were similarly taken from Ref. 40, and the uncertainties were extracted from the original data compilation [41]. Spontaneous fission probability, half-life and atomic weights (the latter two required for the conversion between radionuclide concentration and

activity) are obtained from the JEFF-3.2 library and the latest atomic mass evaluation [32,42]. The data are listed in Table 3, including the activity per unit mass calculated on their basis.

Table 3: Spontaneous fission data and derived activity per unit mass. Uncertainties in atomic weight are $<5 \times 10^{-6}$ %.

| | ^{238}U | ^{232}Th |
|--|-----------------------------------|--------------------------------------|
| Watt fission parameter a (MeV) | 0.6483 | 0.5934 |
| Watt fission parameter b (MeV^{-1}) | 6.811 | 8.030 |
| Atomic weight | 238.051 | 232.038 |
| Branching ratio, $p_{\text{s.f.}}$ | $(5.46 \pm 0.1) \times 10^{-7}$ | $(1.40 \pm 0.5) \times 10^{-11}$ |
| Neutron multiplicity, ν | 2.01 ± 0.03 | 2.14 ± 0.2 |
| Half-life, $T_{1/2}$ (y) | $(4.46799 \pm 0.001) \times 10^9$ | $(1.40503 \pm 0.006) \times 10^{10}$ |
| Activity per unit mass ($\text{Bq } \mu\text{g}^{-1}$) | $80.34 \pm 0.02\%$ | $246.27 \pm 0.4\%$ |

5.2 Decay-induced Neutrons

The spectra of (α, n) neutrons is generally dealt with SOURCES, a code specifically-developed for the determination of neutron production rates and spectra from (α, n) reactions, spontaneous fission and delayed neutron emission due to the decay of various radionuclides [25]. As the original version is restricted to alpha energies up to 6.5 MeV, in-house modifications are developed by some groups to include higher-energy Po descendants ($^{212/216}\text{Po}$ for ^{232}Th and ^{214}Po for ^{238}U).

Alternatively, tabled data can be found in the literature, where secular equilibrium (equal activities) among the various descendants is assumed. Although secular equilibrium applies to naturally occurring ores, it may become significantly altered when specific elements are extracted, either by human or natural processing. Typical examples already found (Table 2) are metals subject to smelting, as well as water and biological materials owing to the reduced solubility of Th in water. The information regarding the descendants is often incomplete, and a reasonable deduction of their activities becomes unfeasible. In such cases secular equilibrium is assumed, and both approaches (SOURCES and tabled data) are equivalent. In this work, we follow the same approach as LUX [23] and use the data from Ref. 43 to obtain

the spectra and production yields of (α,n) neutrons for the SIMPLE material compositions. Although data uncertainties are not reported, a good overall agreement with the literature is mentioned. Based on the uncertainty of this data source [44], a relative uncertainty of 10% is adopted for the total neutron yields, while no values for the spectral distribution itself are considered. This uncertainty value (at $1-\sigma$) is also consistent with the typical agreements found for SOURCES calculations when compared to experiments ($\pm 3\%$ to $\pm 17\%$) [45].

Figure 3 shows the spectra of decay-induced neutrons in different materials of SIMPLE. Table 4 presents the neutron yield per microgram of neutron emitter in the material. For comparison, the values corresponding to spontaneous fission are given. The yield of (α,n) neutrons in BSG is very high, resulting from a significant production in Boron: EXFOR data [32] shows that (α,n) cross sections for ^{10}B and ^{11}B isotopes are in the order of 10^2 mb at the energy range of alphas emitted by ^{238}U and ^{232}Th ($\sim 4\text{-}10$ MeV).

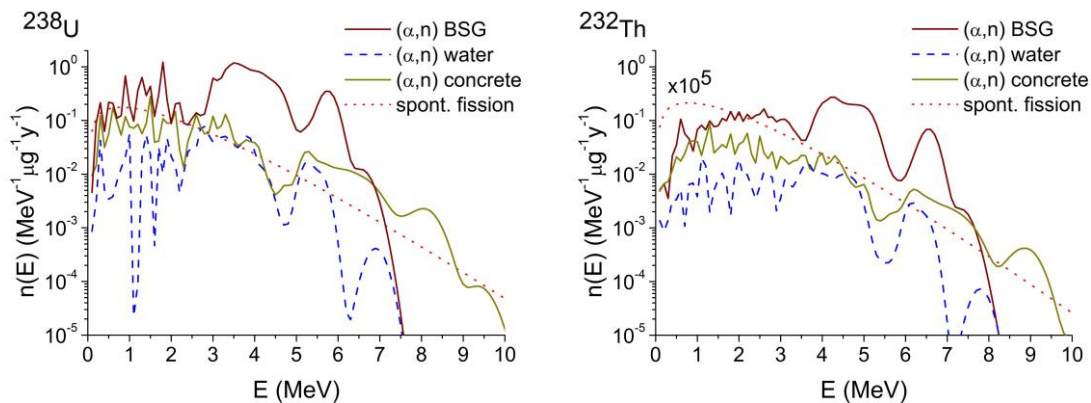


Fig. 3: Spectra of (α,n) neutrons due to the presence of ^{232}Th and ^{238}U in various materials. The Watt distribution representing spontaneous fission neutrons is also represented.

The high relative uncertainty (37%) in the neutron yield from spontaneous fission of ^{232}Th results from the uncertainty in the branching ratio between α -decay and spontaneous fission reported in the evaluated data – which refers to the first measurement of this parameter [46].

For the GRP, we assume that the ^{238}U and ^{232}Th are essentially present in the glass fiber, which corresponds to neglecting their presence in the polypropylene matrix as organic materials generally have high radio-purity. In Table 4 the neutron yields corresponding to interactions in the surrounding matrix and inside the fiber were discriminated. Interactions

with the matrix occur with alphas emitted from the external layers of the roving, at a distance from the surface smaller than range of alphas in E-glass (14-40 μm for 4-8 MeV alphas, as calculated by the SRIM code [47]). Calculations with MCNPX [48] show that the fraction of alpha particles leaving the roving is $(7.8\pm 0.6)\%$ and $(11.2\pm 0.8)\%$ for ^{238}U and ^{232}Th in secular equilibrium, respectively. Only particles with energies > 450 keV were considered. This energy corresponds to the onset of EXFOR (α, n) cross sections in ^{13}C which is the only isotope in the matrix yielding appreciable neutron production for the alpha energies involved. The uncertainties reported originate in the values obtained in the measurement of the roving diameter.

Table 4: Neutron yield (in neutron per microgram of emitter and year) from spontaneous fission and decay-induced (α, n) reactions, due to the presence of ^{238}U and ^{232}Th emitters in the materials. An uncertainty of 10% applies to the (α, n) reaction neutron yields.

| | ^{238}U | ^{232}Th |
|-------------------------|-------------------|------------------------------|
| spontaneous fission | $0.430\pm 2\%$ | $3.84\times 10^{-6}\pm 37\%$ |
| (α, n) reactions | | |
| Rock | 0.137 | 0.0458 |
| Concrete | 0.344 | 0.128 |
| Steel | 0.165 | 0.173 |
| Wood | 0.253 | 0.0766 |
| Water | 0.129 | 0.0403 |
| Paraffin | 0.322 | 0.0964 |
| Polyethylene | 0.324 | 0.0970 |
| Gel | 0.209 | 0.0640 |
| BSG | 2.34 | 0.660 |
| GRP ⁽¹⁾ | 1.63 [0.331-1.74] | 0.506 [0.0994-0.557] |

⁽¹⁾ The lower and upper limits correspond to alpha interactions in the polypropylene and glass fiber, respectively. The adopted value considers a contribution of 88.8% (U) and 92.2% (Th) from (α, n) reactions in E-glass.

6. Neutron Spectrum

Figure 4 shows the calculated neutron spectra for different configurations of GESA: spectra in air prior to the installation of SIMPLE, Phase I and final Stage of Phase II. Each spectrum generally consists of a fast neutron spectrum from the source that is significantly degraded as neutrons scatter on their way to the tallying volume. In this regard, the spectra are essentially similar to that of a moderated nuclear fission reactor, and can be generically described as the combination of a fast Watt, a slowing-down epithermal $1/E$ and a thermal Maxwell distribution. Table 5 summarizes the results concerning thermal (< 0.5 eV) and fast (> 1 MeV) neutron fluence rates in the evaluated configurations.

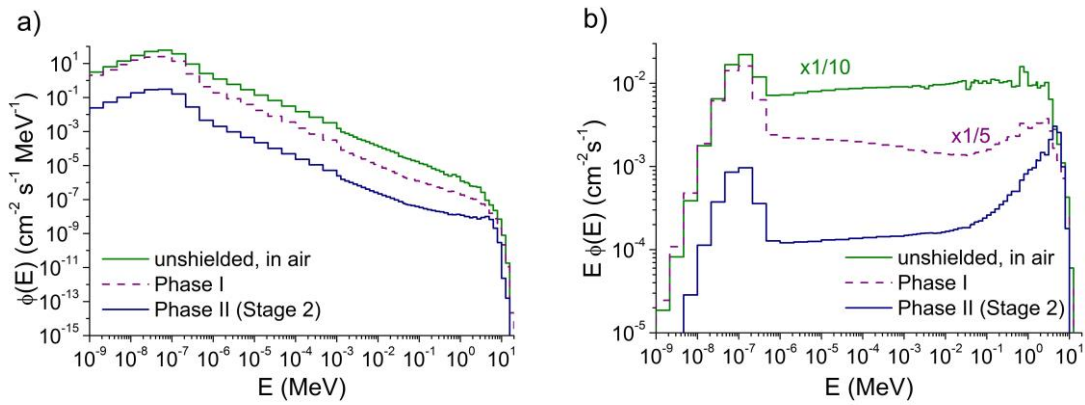


Fig. 4: Calculated neutron spectra for various configurations of GESA
a) representation per unit energy; b) representation per unit lethargy.

Table 5: Thermal and fast neutron fluence rates for various configurations of GESA.

| | $\phi_{\text{thermal}} (\text{cm}^{-2} \text{s}^{-1})$ | $\phi_{\text{fast}} (\text{cm}^{-2} \text{s}^{-1})$ |
|--------------------|--|---|
| unshielded, in air | 5.92×10^{-6} | 1.63×10^{-6} |
| Phase I | 2.12×10^{-6} | 3.03×10^{-7} |
| Phase II (Stage 2) | 2.51×10^{-8} | 3.92×10^{-8} |

The results show that the neutron field intensity decreases 2 orders of magnitude as neutrons traverse the increased moderator thickness used in Phase II. The modification in the neutron spectra caused by the shielding is most evident if one compares the maxima in the thermal (< 0.5 eV) and fast (> 1 MeV) regions using the representation per lethargy (Fig. 4b) commonly used in reactor physics. Relatively to the unshielded configuration (where

$\phi_{\text{fast}}/\phi_{\text{thermal}}=0.28$), there is a noticeable reduction of the fast-to-thermal component in Phase I ($\phi_{\text{fast}}/\phi_{\text{thermal}}=0.143$) due to the small moderator consisting of the SDD gel matrix and tank water. The situation is reversed for the heavily filtered spectrum in Phase II ($\phi_{\text{fast}}/\phi_{\text{thermal}}=1.56$), which is hardened as only the highest-energy neutrons can penetrate through the shielding.

Figure 5 provides further insight of the neutron spectrum for Phase II, with a discrimination of the contributions of various materials and reactions to the overall neutron fluence rate. The water shield effectively reduces the neutron background sources to detector components, the glass container being clearly the major contributor due to the high yield of (α,n) reactions in BSG. In order to improve the accuracy of event rate calculations, a correction of -0.7% is applied to the intensity of the BSG source term that accounts for the mismatch between the calculated and measured container masses.

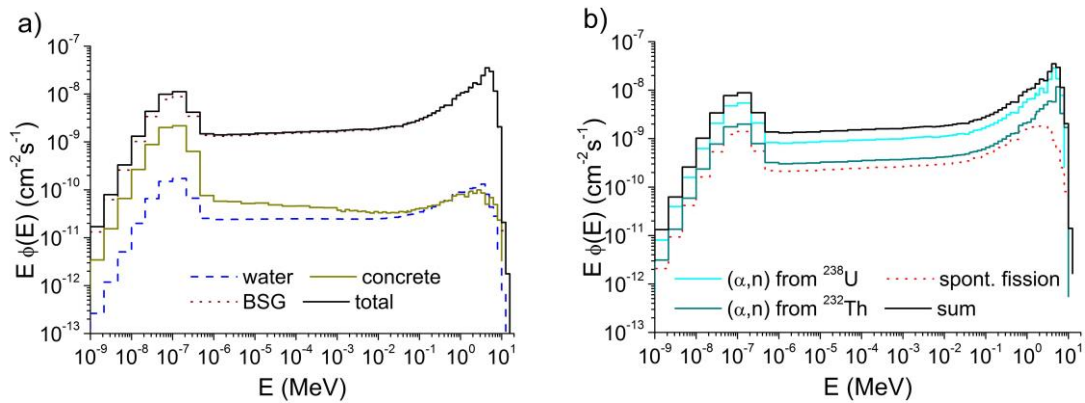


Fig. 5: Calculated on-detector neutron spectra for Stage 2 of SIMPLE Phase II discriminating a) selected material contributions and b) neutron-producing reactions in BSG.

7. Event Rates

7.1 Reactions

The E_{crit} and LET_{crit} thresholds referred to in Section 1 determine the minimum nuclear recoil energy (E_{rec}) for the production of a bubble nucleation. For the particles of interest (neutrons and nuclear recoils) the LET can be considered equal to the stopping power, i.e. *bremmstrahlung* radiation and secondary electrons (delta-rays) are neglected. Stopping powers calculated by SRIM [47] were used to extract E_{rec} .

Neutron scattering (elastic and inelastic) were scrutinized as event-producing sources, as well as transmutation reactions with positive Q-values: (n,p) and (n, α) in ^{35}Cl . The relation between nuclear recoil and neutron energies is defined by standard kinematic equations [49] involving the reaction Q-value, particle's atomic weights and the angular deviation upon interaction. For each reaction, the minimum neutron energy yielding a nucleation (E_{\min}) was derived for head-on collisions corresponding to the maximum energy transfer.

The values of E_{rec} and E_{\min} are presented in Table 6, for the various reactions considered. With respect to inelastic scattering: the data refers to the first excited state, which has smaller $|Q|$ hence is more populated.

Table 6: Minimum nuclear recoil (E_{rec}) and neutron (E_{\min}) energies for the production of a nucleation in C_2ClF_5 .

| Reaction | Q-value (keV) | E_{rec} (keV) | E_{\min} (keV) | Isotopic abundance (%) |
|---|-----------------------|---|---------------------|---------------------------|
| Elastic scattering | | | | |
| $^{12}\text{C}(n,n)^{12}\text{C}$ | 0 | 115 | 402 | 98.93 \pm 0.088 |
| $^{13}\text{C}(n,n)^{13}\text{C}$ | | 123 | 460 | 1.07 \pm 0.08 |
| $^{19}\text{F}(n,n)^{19}\text{F}$ | | 8 | 43 | 100 |
| $^{35}\text{Cl}(n,n)^{35}\text{Cl}$ | | 8 | 75 | 75.76 \pm 0.10 |
| $^{37}\text{Cl}(n,n)^{37}\text{Cl}$ | | 8 | 79 | 24.24 \pm 0.10 |
| Inelastic scattering | | | | |
| $^{12}\text{C}(n, n_1')^{12}\text{C}$ | -4438.91 \pm 0.31 | 115 | 4812 | 98.93 \pm 0.088 |
| $^{13}\text{C}(n, n_1')^{13}\text{C}$ | -3089.443 \pm 0.020 | 123 | 3329 | 1.07 \pm 0.08 |
| $^{19}\text{F}(n, n_1')^{19}\text{F}$ | -109.894 \pm 0.05 | 8 | 120 | 100 |
| $^{35}\text{Cl}(n, n_1')^{35}\text{Cl}$ | -1219.29 \pm 0.11 | 8 | 1255 | 75.76 \pm 0.10 |
| $^{37}\text{Cl}(n, n_1')^{37}\text{Cl}$ | -1726.58 \pm 0.04 | 8 | 1774 | 24.24 \pm 0.10 |
| Transmutation reactions with Q>0 | | | | |
| $^{35}\text{Cl}(n,p)^{35}\text{S}$ | 615.0234 \pm 0.0532 | ^{35}S :8 | 0 | 75.76 \pm 0.10 |
| $^{35}\text{Cl}(n,\alpha)^{32}\text{P}$ | 937.74 \pm 0.05 | ^{32}P : 8; α : 269-1981 | 0 | 75.76 \pm 0.10 |

Heavy recoiling nuclei (F, Cl, S, P) have high LET, and the constraint in E_{rec} is determined by E_{crit} ; in contrast, for lighter particles such as C nuclei, E_{rec} is set by LET_{crit} .

The transmutation reactions in ^{35}Cl can induce a nucleation regardless of neutron energy, because $Q > 0$ and the heavier reaction products emerge with energy larger than 17 keV (^{35}S) and 104 keV (^{32}P). A similar effect occurs for the recoiling nuclei from inelastic scattering in C and Cl (for neutron energies above the reaction threshold, since $Q < 0$) which emerge with minimum energies of 344 keV (^{12}C), 34 keV (^{35}Cl) and 46 keV (^{37}Cl); the minimum neutron energies in Table 5 are therefore equal to the reaction thresholds. The recoiling nucleus from inelastic scattering in F emerges with the minimum energy of 5.5 keV which is lower than the E_{rec} ; in this case E_{min} is larger than the reaction threshold energy.

7.2 Cross Sections

Table 5 displays differences between the isotopes of C and Cl with respect to E_{min} . For the event rate calculations some simplifications were introduced based on the reaction cross sections, with a selection shown in Fig. 6.

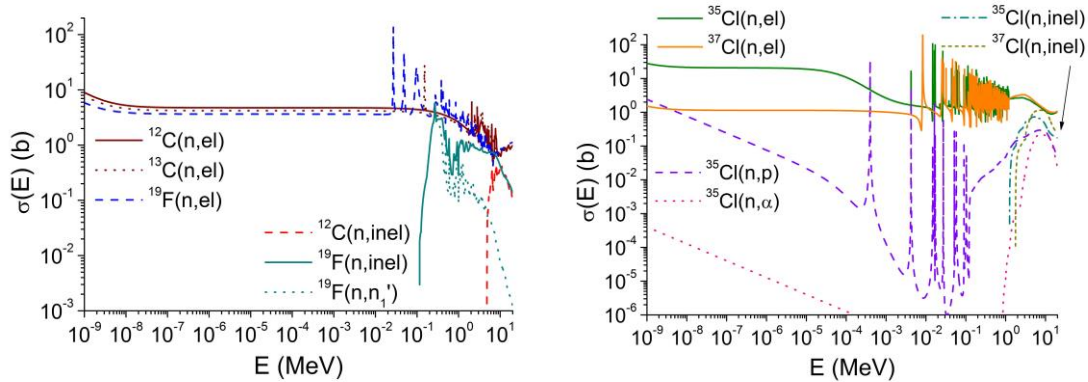


Fig. 6: Cross sections of selected neutron reactions originating events in SIMPLE SDDs. The data is taken from the ENDF-B7.1 library, except for ^{12}C (CENDL-3.1) and ^{13}C (JEFF-3.2) [32]. Labels (n,el) and (n,inel) refer to total elastic and total inelastic scattering, respectively.

7.3 Conversion of Neutron Fluence to Event Rates

The event rate (R) per target atom due to each nucleation-inducing reaction is generically calculated as $R = \int \sigma(E)\eta(E)\phi(E) dE$, where η is the nucleation efficiency, described as

$\eta(E) = 1 - \exp[-\Gamma(E/E_{\min} - 1)]$ for $E \geq E_{\min}$ (and 0 otherwise) with $\Gamma=4.2\pm 0.3$ [1]. With MCNP output group fluence rates, the event rate (R) due to each reaction can be calculated as a sum over the various energy bins:

$$R = \sum_i N \langle \sigma \rangle_i \langle \eta \rangle_i \phi_i \quad (1)$$

where N is the number of target atoms, ϕ is the calculated group neutron fluence rate, $\langle \sigma \rangle_i$ and $\langle \eta \rangle_i$ are the spectral-averaged values of the reaction cross section intrinsic and nucleation efficiency in the i^{th} energy bin.

The spectral-averaged group cross sections and efficiencies were calculated using FLXPRO. The original pointwise-evaluated cross section data was initially converted to the standard SAND-II 640 group structure (45 equi-lethargy groups per decade from 1 meV to 1 MeV and group width of 100 keV for 1 - 20 MeV) [50] with a flat weighting spectrum. These fine group cross sections were later converted to the group structure of the simulations using a reactor weighting spectrum consisting of a Maxwell, 1/E and Watt distributions. Nucleation efficiencies were input in the SAND-II structure.

The contribution of elastic scattering on ^{13}C in the energy interval 402-460 keV has not been discriminated because this is a minor isotope with slightly smaller cross section than that of ^{12}C ; the cross section of natural C was used above 402 keV. The cross section of natural Cl was used beyond 75 keV to describe elastic scattering, as its two isotopes have similar energy thresholds and the contribution of ^{37}Cl is simultaneously decreased since it is the less abundant and has the smaller cross section.

The data in Table 6 for inelastic scattering refers to the first excited state. Although total inelastic cross sections are significantly larger, the states of higher orders have increased E_{\min} yielding the corresponding event rates smaller than inferred by cross section ratios. The total inelastic cross section starts to deviate from the one for the first excited state at ~ 2 MeV (Cl), 5 MeV (C) and 10 MeV (F) where SDDs have a decreased neutron population. As a first approximation, inelastic scattering was dealt with by considering E_{\min} for the first excited state and the total inelastic cross section, thereby providing an upper limit to its contribution.

8. Results

Table 7 shows the calculated event rates considering maximum energy transfer. The contribution of the various neutron-producing reactions is discriminated. In the case of GRP, values corresponding to (α,n) interactions in the polypropylene matrix (lower value) and in the glass fiber are given; a weighted average is reported in the sum considering that the relative contribution of the alpha interactions occur within the glass fiber (Section 5.2).

The results are organized in 3 groups: (i) the structural materials of the facility; (ii) materials added to shield against neutrons; (iii) materials used to set-up the detector. In contrast to the structural materials, both the external shield and the detector materials may be subject to modification in future SIMPLE developments.

Various results correspond to upper limits that reflect the experimental detection limits regarding the radio-assays. With the concrete shielding neutrons from the rock, the upper limits reported for the later reflect the use of the shallowest concrete layer in the simulations. Due to its negligible contributions to the total event rate, these upper limits are not subject to more refined analysis.

The results suggest that most of the detector background signal is created by the detector container of BSG (87%) and to a lesser degree by the tank GRP walls (12%). The contribution of the structural materials (mostly from the concrete) is reduced to 0.7% and the external shielding (essentially the water) contributes with less than 0.2% to the background.

The energy distribution of the recoils was calculated for elastic and inelastic scattering, the only event-producing reactions available within SPECTER. The recoil spectrum for each reaction was normalized to the respective reaction rate, and folded with the efficiency curve in order to determine the number of recoils with energies larger than E_{\min} . Figure 7 shows the energy distribution of the recoils and Table 8 presents the calculated event rates, discriminating the event-inducing reactions in C_2ClF_5 . There is a clear predominance (56%) of elastic scattering in fluorine that results from its large abundance in the superheated liquid, and a residual contribution (1%) of the transmutation reactions in the Cl isotopes due to their reduced cross sections.

Table 7: Calculated event rates for maximum energy transfer and final value considering the angular distribution of the recoiling nuclei.

| Neutron origin | Event rate (evt/kg-d) | | | |
|--------------------------|------------------------|---|---|------------------------|
| | s.f. | (α ,n) from ^{238}U | (α ,n) from ^{232}Th | Sum |
| (i) Structural materials | | | | |
| Rock | $<4.66 \times 10^{-7}$ | $<2.88 \times 10^{-6}$ | $<7.30 \times 10^{-9}$ | $<3.55 \times 10^{-6}$ |
| Concrete | 9.38×10^{-4} | 1.33×10^{-3} | 1.13×10^{-3} | 3.40×10^{-3} |
| Steel | 1.21×10^{-8} | 2.59×10^{-9} | 4.03×10^{-9} | 1.88×10^{-8} |
| Wood | 2.21×10^{-6} | 5.88×10^{-6} | 1.38×10^{-7} | 8.23×10^{-6} |
| (ii) Shield | | | | |
| Water-external shield | 3.29×10^{-4} | 1.71×10^{-4} | 2.64×10^{-7} | 5.00×10^{-4} |
| Paraffin | $<3.71 \times 10^{-8}$ | $<3.30 \times 10^{-7}$ | $<4.51 \times 10^{-7}$ | $<8.18 \times 10^{-7}$ |
| Polyethylene | 1.75×10^{-5} | 6.54×10^{-5} | 5.26×10^{-5} | 1.36×10^{-4} |
| (iii) Intrinsic | | | | |
| GRP ⁽¹⁾ | 3.60×10^{-3} | $[5.16 \times 10^{-3} - 1.73 \times 10^{-2}]$ | $[9.80 \times 10^{-3} - 4.01 \times 10^{-2}]$ | 5.66×10^{-2} |
| Water-tank | 1.44×10^{-3} | 5.84×10^{-4} | 8.78×10^{-7} | 2.03×10^{-3} |
| BSG | 4.74×10^{-2} | 2.64×10^{-1} | 1.02×10^{-1} | 4.13×10^{-1} |
| Gel | $<3.87 \times 10^{-4}$ | $<1.50 \times 10^{-4}$ | - | $<5.38 \times 10^{-4}$ |
| Microphone | $<1.97 \times 10^{-4}$ | $<7.55 \times 10^{-5}$ | - | $<2.72 \times 10^{-4}$ |
| Total | | | | 4.77×10^{-1} |

⁽¹⁾ The lower and upper limits correspond to alpha interactions in the polypropylene and in the glass fiber, respectively. The adopted value considers a contribution of 88.8% (U) and 92.2% (Th) from (α ,n) reactions in E-glass.

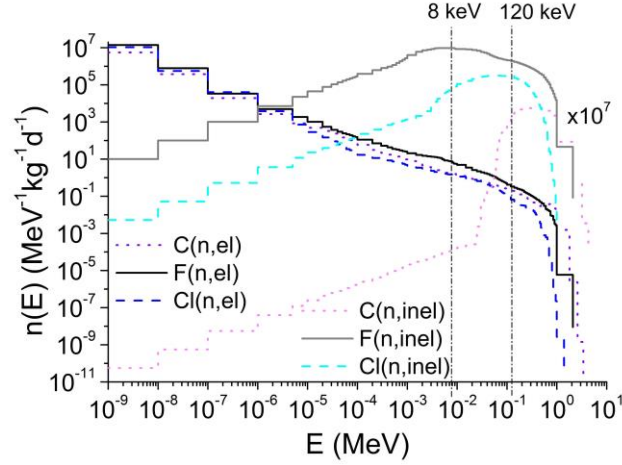


Fig. 7: Energy distribution of the recoil nuclei. The 10^7 factor applies to all inelastic scattering curves. The vertical lines locate the E_{rec} thresholds for Cl and F (8 keV), as well as C (120 keV), below which no events are induced.

Table 8: Contribution of the various event-producing reactions to the detector signal. The last column provides the final result when the energy distribution of the recoiling nuclei, obtained by considering the angular effects, is included. The statistical uncertainty for each reaction varies between 0.6% and 1.1%.

| Reaction | Event rate (evt/kg-d) | |
|---|--------------------------------------|----------------------------|
| | Maximum energy transfer | Recoil energy distribution |
| C(n,el) | 6.45×10^{-2} | 3.71×10^{-2} |
| Cl(n,el) | 4.37×10^{-2} | 4.25×10^{-2} |
| F(n,el) | 2.66×10^{-1} | 2.10×10^{-1} |
| $^{35}\text{Cl}(n,p) \text{ } ^{35}\text{S}$ | 5.42×10^{-2} | - |
| $^{35}\text{Cl}(n,\alpha) \text{ } ^{32}\text{P}$ | 4.33×10^{-4} | - |
| C(n,inel) | 3.92×10^{-4} | 3.83×10^{-4} |
| F(n,inel) | $8.91 \times 10^{-2} \text{ }^{(1)}$ | 7.10×10^{-2} |
| Cl(n,inel) | 6.48×10^{-3} | 6.44×10^{-3} |
| Total | 4.76×10^{-1} | 3.67×10^{-1} |

⁽¹⁾ Includes the correction for the simplified cross section treatment.

With inelastic scattering in F corresponding to 19% of the detector signal, evaluation of the resulting error by the simplified treatment (Section 6.2) is pertinent. An accurate calculation was performed for fluorine considering 21 excited states and the total neutron spectrum. The contribution of the excited states to the total F(n,inel) event rate is 29% (n_1'), 49% (n_2'), 6% (n_3' and n_4'), 9% (n_5'), 1% (n_6') and less than 0.3% for each of the higher order states. This detailed calculation yielded 98.3% of the value previously determined: a correction of -1.7% is applied, which explains the small discrepancy between the total event rate in Tables 7 and 8.

The calculated background event rate in Stage 2 of SIMPLE is 0.367 evt/kgd. This value is 10% larger than previously reported [1, 30] by virtue of the increase by the introduction of neutron emission by the tank walls (+14%) and the inelastic scattering (+26%) that is counterbalanced (-23%) by the angular effects.

8.1 Uncertainty Analysis

The statistical uncertainties in the group fluence rates were kept below 10% for each bin by simulating a sufficiently large number of source particles and employing variance reduction techniques available in MCNP when necessary. The propagated statistical uncertainty in the event rate is 0.51%. The precision of the results is therefore limited by the non-statistical uncertainties, most of which are related to the measurement uncertainty in the radio-assays and have been indicated previously. The missing contributions are addressed as follows.

a) Cross section data

The uncertainty associated to the reaction cross sections was evaluated using the FLXPRO code to convert their variances from the original evaluated data to the BUGLE group structure of the calculated neutron spectrum. The analysis was applied to the principal contributing reactions, yielding relative uncertainties of 1.8% and 3.1% for elastic and inelastic scattering in F and 0.34% for elastic scattering on C.

b) Inelastic scattering

Inelastic scatterings in C and Cl have modest contributions to the detector signal (0.1% for C; 2% for Cl): their simplified treatment is not subject to finer analyses. Based on the

correction of 1.7% calculated for F, we attribute a conservative uncertainty of 5% to the calculated values for C and Cl.

c) Material composition

BSG and GRP have important contributions to the background signal due to their high Boron content in combination with considerable amounts of α -emitting radio-impurities. The measurement uncertainty for the B content in BSG is 4%, in the case of GRP, for which a nominal composition was used, an uncertainty of 10% ($1-\sigma$) is considered reflecting the range of variability in the reference data. The uncertainty of the weight factors, attributed to the contributions of (n,α) reactions in the E-glass and the embedding polypropylene, is estimated as 7.2% and represents the uncertainty in the roving diameter.

d) Nucleation efficiency

The uncertainty associated with the Γ factor employed in the efficiency curve was determined by repeating the calculations for elastic and inelastic scattering in F with the extreme values of 3.9 and 4.5 (Section 7.3). The variation in the sum of the corresponding event rates was 0.6%.

e) Simulation

Any simulation code has inherent inaccuracies due to, for example the transport cross sections and the interaction models. In addition, there are unavoidable errors in the geometry description or material composition of such a complex and large set-up such as SIMPLE. This is particularly relevant for neutron transport, being strongly influenced by the interacting elements and isotopes. As shown in previous studies, e.g. Refs. 51, 52, discrepancies of 10% between absolute neutron simulation and experiment are common. This value is adopted as an estimate of the uncertainty associated with the simulation procedure.

f) Muon-induced neutrons

The interaction of cosmic muons with rock generates high energy neutrons that emerge from the cavern surface and contribute to the detector signal. This contribution was estimated using MCNPX considering a surface neutron source at GESA's ceiling. The neutron energy distribution above 10 MeV was extracted from Ref. 53. Since the neutron distribution depends on the muon energies involved, the required parameters were

averaged over the muon spectrum expected at GESA's depth. Group fluence rates and angular distributions from Ref. 54 were used to complete the characterization of the source. The estimated group fluence rates in GESA were interpolated from the data for other facilities considering their depth, as well as the density and average mass number of the rock (23.4 for GESA). Reaction cross sections from JENDL-HE-2007 [32] were used to calculate the event rates. As shown in Table 9, the estimated muon-induced event rate is 1.8×10^{-3} evt/kgd, corresponding to 0.5% of the total value.

Table 9: Estimated muon-induced recoil event rates. Monoenergetic neutrons with the maximum group energy were considered at ≤ 10 MeV (two lowest energy groups).

| Neutron energy | Fluence rate ($10^{-9} \text{ cm}^{-2} \text{ s}^{-1}$) | Event rate (10^{-4} evt/kgd) |
|----------------|--|---|
| 0 – 1 MeV | 26 | ~0 |
| 1 – 10 MeV | 2.7 | 0.17 |
| 10 – 100 MeV | 8.0 | 8.8 |
| 0.1 – 3 GeV | 1.9 | 8.7 |

In Table 10 an uncertainty analysis is presented considering the non-statistical uncertainties. Uncertainties of 100% have been associated with quantities lacking a reliable uncertainty estimate. The sensitivity coefficients (i.e., the relative contribution of each quantity to the total event rate) is included to derive the propagated uncertainty. Only values yielding relative uncertainties larger than 0.1% are shown.

The results show that the largest identified uncertainties are associated with the tabled (α, n) yields, the experimental uncertainty in quantification of U in BSG and the simulation procedure – their combination yielding essentially the overall uncertainty of 17.4%.

The final estimate for the calculated background event rate in Stage 2 of SIMPLE is $0.367 \pm 0.002(\text{stat.}) \pm 0.064$ (non-stat.) evt/kgd, or a 10% increase in the anticipated recoil background estimate, which insignificantly changes the Feldman-Cousins analysis of the contribution to the overall Phase II measurements.

Table 10: Uncertainties ($1-\sigma$) in the calculated background event rate. Only values yielding propagated uncertainties larger than 0.1% are presented.

| Quantity | Uncertainty (%) | Origin of uncertainty | Sensitivity coeff. (%) | Propagated uncert. (%) |
|-------------------------------|-----------------|---------------------------|------------------------|------------------------|
| Statistical | 0.51 | simulation statistics | 100 | 0.51 |
| Non-statistical | | | | |
| (α,n) yield | 10 | reported accuracy | 87.7 | 8.8 |
| F(n,el+inel) react. Rate | 0.57 | nucleation efficiency | 74.7 | 0.43 |
| F(n,el) react. rate | 1.8 | cross section data | 55.7 | 1.0 |
| F(n,inel) react. rate | 3.1 | cross section data | 19.0 | 0.59 |
| | 1.7 | simplified calculation | 19.0 | 0.32 |
| U in BSG | 15 | measurement | 69.7 | 10.4 |
| Th in BSG | 8.7 | | 22.8 | 2.0 |
| U in GRP | 6.3 | | 4.46 | 0.28 |
| Th in GRP | 10.6 | | 1.36 | 0.14 |
| U in water | 100 | non-equilibrium | 0.69 | 0.69 |
| B in BSG | 4.0 | measurement | | |
| B in GRP | 10 | nominal composition | 5.02 | 0.50 |
| MCNP output | 10 | model inaccuracies | 100 | 10 |
| Muon-induced neutrons | 0.48 | estimated contribution | 100 | 0.48 |
| Others, non-statistical | | | | 0.11 |
| Combined relative uncertainty | | | | 17.4 |

9. Perspectives for SIMPLE Phase III

Improved background reduction is essential for the next phase of SIMPLE using bubble chamber prototypes in GESA [55]. The approach consists of (i) replacing the BSG and GRP containers by materials with increased radio-purity and composition; (ii) employing purified water in the shielding and (iii) increasing the water thickness to shield against the concrete. Candidate materials for the containers (organic and boron-free) have been evaluated by NAA

with respect to the ^{238}U content, yielding $<0.424 \text{ Bq kg}^{-1}$ (detector) and $<0.673 \text{ Bq kg}^{-1}$ (tank); for demineralized water, alpha spectroscopy has determined $1.8 \times 10^{-4} \text{ Bq l}^{-1}$ of ^{238}U and $3.4 \times 10^{-5} \text{ Bq l}^{-1}$ of ^{232}Th . From a scaling of the current results to these values, a background signal $<10^{-2} \text{ evt/kgd}$ is estimated, originating mostly in the detector container (the tank walls and shielding water contributing with $<5 \times 10^{-4} \text{ evt/kgd}$ and $<2 \times 10^{-5} \text{ evt/kgd}$, respectively). The upper limits should be overcome via radio-assays at lower detection limits, e.g. by low background photon spectroscopy or inductively coupled plasma mass spectroscopy (ICPMS) for a science run. Once these radio-purity requirements are achieved, the muon-induced neutron signal is expected to become the principal background contributor. Further developments will demand a much larger water shield (thickness of various meters) to attenuate the high energy neutrons ($>100 \text{ MeV}$) or the relocation of the experiment to larger depth.

10. Conclusions

The estimated SDD neutron background signal for Stage 2 of SIMPLE Phase II was simulated using the MCNP code, yielding $0.367 \pm 0.002(\text{stat.}) \pm 0.064 \text{ (non-stat.) evt/kgd}$. For the net exposure of 6.71 kgd in Stage 2 this corresponds to 2 estimated events vs. 1 measured.

The uncertainties associated to the (α, n) yields and the simulation itself set a minimum value of 13% for the non-statistical uncertainty; the measurement uncertainty of U in the BSG is the main cause to exceeding this value.

Next developments in SIMPLE depend on reducing the neutron background using Boron-free materials and increased radio-purity. Promising candidates that have been identified should be assayed using techniques with lower detection limits (ICPMS, low-level spectroscopy).

With a reduction of the intrinsic background by two orders of magnitude relatively to Phase II, muon-induced neutrons are expected to become important contributors to the SDD signal. A transition from MCNP to FLUKA or GEANT is anticipated in order to assess the neutron background in future SIMPLE experiments.

Acknowledgements

We thank Daniel Boyer, Alain Cavaillou and Michel Auguste (LSBB) for their assistance in the Stage 2 shielding, and provision of the additional materials samples assayed in this report. We also thank Harry Miley and Rosey Payne (PNNL), Pia Loaiza (LSM) and Christophe Destouches (Univ. Avignon) for the radio- and chemical assays of the GESA construction materials.

We are grateful to Dr. Larry Greenwood from Argonne National Laboratory for providing the full version of the SPECTER code, as also Luís Alves (C2TN) for the microscope usage.

This work was supported by Grants PDTC/FIS/115733/2009 and PDTC/FIS/121130/2010 of the Portuguese Foundation for Science and Technology (FCT). The activity of M. F. was supported by Grant SFRH/BD/46545/2008 of the FCT.

References

- [1] M. Felizardo, T. A. Girard, T. Morlat *et al.*, The SIMPLE Phase II dark matter search, *Physical Review* **D89** (2014) 072013-p.1–20. doi: 10.1103/PhysRevD.89.072013
- [2] S. Archambault, E. Behnke, P. Bhattacharjee *et al.*, Constraints on Low-Mass WIMP Interactions on ^{19}F from PICASSO, *Physics Letters* **B711** (2012) 153–161. doi: 10.1016/j.physletb.2012.03.078
- [3] E. Behnke, J. Behnke, S. J. Brice *et al.*, First dark matter search results from a 4-kg CF3I bubble chamber operated in a deep underground site, *Physical Review* **D86** (2012) 052001-p.1–9. doi: 10.1103/PhysRevD.86.052001
- [4] C. Amole, M. Ardid, D.M. Asner *et al.*, Dark matter search results from the PICO-2L C3F8 bubble chamber. arXiv: 1503.00008v1
- [5] R.E. Apfel, The superheated drop detector, *Nuclear Instruments and Methods* **162** (1979) 603–608.
- [6] F. Seitz, On the theory of the bubble chamber, *Physics of Fluids* **1** (1958) 2–13.
- [7] M. Felizardo, R.C. Martins, A.R. Ramos *et al.*, New acoustic instrumentation for the SIMPLE superheated droplet detector, *Nuclear Instruments and Methods in Physics Research* **A589** (2008) 72–84. doi: 10.1016/j.nima.2008.02.012

- [8] M. Felizardo, T. Morlat, A. C. Fernandes *et al.*, First results of the Phase II SIMPLE dark matter search, *Physical Review Letters* **105** (2010) 211301-p.1–4.
doi: 10.1103/PhysRevLett.105.211301
- [9] T.A. Girard, M. Felizardo, A.C. Fernandes, J.G. Marques and A.R. Ramos, Girard *et al.* (for the SIMPLE collaboration) reply (to C. E. Dahl *et al.*, preceding Comment, *Phys. Rev. Lett.* **108**, 259001 (2012)), *Physical Review Letters* **108** (2012) 259002-p.1–2.
doi: 10.1103/PhysRevLett.108.259002
- [10] X-5 Monte Carlo Team, MCNP: A General N-Particle Transport Code (Version 5) Vol. 1, LA-UR-03-1987, Los Alamos National Laboratory, 2003.
- [11] J. Allison, K. Amako, J. Apostolakis *et al.*, Geant4 developments and applications, *IEEE Transactions on Nuclear Science* **53** (2006) 270–278.
doi: 10.1109/TNS.2006.869826
- [12] T.T. Böhlen, F. Cerutti, M.P.W. Chin, A. Fassò, A. Ferrari, P.G. Ortega, A. Mairani, P.R. Sala, G. Smirnov and V. Vlachoudis, The FLUKA Code: Developments and challenges for high energy and medical applications, *Nuclear Data Sheets* **120** (2014) 211–214. doi: 10.1016/j.nds.2014.07.049.
- [13] S. Archambault, F. Aubin, M. Auger *et al.*, Optimization of neutron shielding for the PICASSO experiment, *AIP Conference Proceedings* **1180** (2009) 112–116.
- [14] R. Agnese, Z. Ahmed, A. J. Anderson *et al.*, Silicon Detector Dark Matter Results from the Final Exposure of CDMS II, *Physical Review Letters* **111** (2013) 251301-p.1–6.
doi: 10.1103/PhysRevLett.111.251301.
- [15] E. Aprile, M. Alfonsi, K. Arisaka *et al.*, The neutron background of the XENON100 dark matter search experiment, *Journal of Physics* **G40** (2013) 115201-p.1–17.
doi: 10.1088/0954-3899/40/11/115201
- [16] V.A. Kudryavtsev, M. Robinson and N.J.C. Spooner, The expected background spectrum in NaI dark matter detectors and the DAMA result, *Astroparticle Physics* **33** (2010) 91–96. doi: 10.1016/j.astropartphys.2009.12.003.
- [17] H.M. Araújo, D.Yu. Akimov, E.J. Barnes *et al.*, Radioactivity backgrounds in ZEPLIN–III. *Astroparticle Physics* **35** (2012) 495–502. doi: 10.1016/j.astropartphys.2011.11.001
- [18] H.R.T. Wulandari, Study on neutron-induced background in the dark matter experiment CRESST, PhD thesis, Technischen Universität München, 2003.
- [19] E. Armengaud, C. Augier, A. Benoit *et al.*, Background studies for the EDELWEISS dark matter experiment, *Astroparticle Physics* **47** (2013) 1–9.
doi: 10.1016/j.astropartphys.2013.05.004.

- [20] C.E. Aalseth, P.S. Barbeau, J. Colaresi *et al.*, CoGeNT: A Search for Low-Mass Dark Matter using p-type Point Contact Germanium Detectors, *Physical Review* **D88** (2013) 012002-p.1–20. doi: 10.1103/PhysRevD.88.012002
- [21] D.A. Fustin, First Dark Matter Limits from the COUPP 4 kg Bubble Chamber at a Deep Underground Site, PhD thesis, University of Chicago, 2012
- [22] H. Uchida, K. Abe, K. Hieda *et al.*, Search for inelastic WIMP nucleus scattering on ^{129}Xe in data from the XMASS-I experiment, *Progress of Theoretical and Experimental Physics* **6** (2014), 063C01-p.1–11. doi: 10.1093/ptep/ptu064
- [23] D.S. Akerib, H.M. Araújo, X. Bai *et al.*, Radiogenic and Muon-Induced Backgrounds in the LUX Dark Matter Detector, *Astroparticle Physics* **62** (2015) 33–46. doi: 10.1016/j.astropartphys.2014.07.009
- [24] H.J. Kim, I.S. Hahn, M.J. Hwang *et al.*, Measurement of the neutron flux in the CPL underground laboratory and simulation studies of neutron shielding for WIMP searches, *Astroparticle Physics* **20** (2004) 549–557. doi: 10.1016/j.astropartphys.2003.09.001
- [25] W.B. Wilson, R.T. Perry, W.S. Charlton, T.A. Parish and E.F. Shores, Sources: A code for calculating (α, n), spontaneous fission, and delayed neutron sources and spectra, *Radiation Protection Dosimetry* **115** (2005) 117–121. doi: 10.1093/rpd/nci260
- [26] S.A. Pozzi, E. Padovani and M. Marseguerra, MCNP-PoliMi: a Monte-Carlo code for correlation measurements, *Nuclear Instruments and Methods in Physics Research* **A513** (2003) 550–558. doi: 10.1016/j.nima.2003.06.012
- [27] M. Felizardo, T.A. Girard, T. Morlat *et al.*, Final analysis and results of the Phase II SIMPLE dark matter search, *Physical Review Letters* **108** (2012) 201302-p.1–5. doi: 10.1103/PhysRevLett.108.201302
- [28] LSBB, <http://lsbb.oca.eu>
- [29] T.A. Girard, F. Giuliani, T. Morlat *et al.*, SIMPLE dark matter search results, *Physics Letters* **B621** (2005) 233–238. doi:10.1016/j.physletb.2005.06.070.
- [30] A.C. Fernandes, M. Felizardo, A. Kling, J.G. Marques and T. Morlat, Studies on the efficiency of the neutron shielding for the SIMPLE dark matter search, *Nuclear Instruments and Methods in Physics Research* **A623** (2010) 960–967. doi:10.1016/j.nima.2010.07.044.
- [31] F.W. Stallmann, LSL-M2: a computer program for least-squares logarithmic adjustment of neutron spectra, NUREG/CR-4349, ORNL/TM-9933, Oak Ridge National Laboratory, 1985.

- [32] Evaluated nuclear data available from the Nuclear Energy Agency at <http://www.oecd-neo.org/janisweb/search/endl>
- [33] L. R. Greenwood and R. K. Smither, SPECTER: Neutron Damage Calculations for Materials Irradiations, ANL/FPP/TM-197, Argonne National Laboratory, 1985.
- [34] F.T. Wallenberger, J.C. Watson and H. Li, Glass fibers, in: D.B. Miracle and S.L. Donaldson (Eds.), Composites, ASM Handbook Vol. 21 (American Society for Metals International, Materials Park OH, 2001), pp. 27–34. ISBN 978-0-87170-703-1
- [35] B.S. Hayes and L.M. Gammon, Composite materials and optical microscopy, Chapter 1 in: Optical microscopy of fiber-reinforced composites (American Society for Metals International, Materials Park OH, 2010) pp. 1–22. ISBN 978-1-61503-044-6
- [36] M. Felizardo, T. Morlat, J.G. Marques, A.R. Ramos, TA Girard, A.C. Fernandes, A. Kling, I. Lázaro, R.C. Martins and J. Puibasset, Fabrication and response of high concentration SIMPLE superheated droplet detectors with different liquids, *Astroparticle Physics* **49** (2013) 28–43. doi: 10.1016/j.astropartphys.2013.08.006
- [37] Rousselot gelatin. http://www.parmentier.de/gpfneu/gelatine/rousselot_en.pdf
- [38] Duran laboratory glassware.
<http://www.us.schott.com/labware/english/products/duran/onlinecatalogue/index.html>
- [39] R.C. Pettersen, The chemical composition of wood, Chapter 2 in: R.M. Rowell (Ed.), The Chemistry of Solid Wood, Advances in Chemistry Series Vol. 27 (American Chemical Society, Washington DC, 1984) pp. 57–126.
doi: 10.1021/ba-1984-0207.ch002
- [40] E.F. Shores, Data updates for the SOURCES-4A computer code, *Nuclear Instruments and Methods in Physics Research* **A179** (2001) 78–82.
doi:10.1016/S0168-583X(00)00694-7.
- [41] F. Manero and V.A. Konshin, Status of the energy-dependent ν -values for the heavy isotopes ($Z > 90$) from thermal to 15 MeV and of ν -values for spontaneous fission, *Atomic Energy Review* **10** (1972) 638–756.
- [42] M. Wang, G. Audi, A.H. Wapstra, F.G. Kondev, M. MacCormick, X. Xu and B. Pfeiffer, The AME2012 atomic mass evaluation, *Chinese Physics* **C36** (2012) 1603–2014.
- [43] D.-M. Mei, C. Zhang and A. Hime, Evaluation of (α, n) induced neutrons as a background for dark matter experiments, *Nuclear Instruments and Methods* **A606** (2009) 651–660. doi:10.1016/j.nima.2009.04.032.
Data available at <http://neutronyield.usd.edu>.

- [44] R. Heaton, H. Lee, P. Skensved and B.C. Robertson, Neutron production from thick-target (α, n) reactions. *Nuclear Instruments and Methods* **A276** (1989) 529–538. doi:10.1016/0168-9002(89)90579-2.
- [45] W.B. Wilson, R.T. Perry, E.F. Shores, *et al.*, SOURCES 4C: A code for calculating (α, n), spontaneous fission, and delayed neutron sources and spectra. LA-UR-02-1839, Los Alamos National Laboratory, 2002.
- [46] R. Bonneti, C. Chiesa, A. Guglielmetti, R. Matheoud, G. Poli, V.L. Mikheev, S.P. Tretyakova. First observation of spontaneous fission and search for cluster decay of Th-232, *Physical Review* **C51** (1995) 2530–2533. doi: 10.1103/PhysRevC.51.2530
- [47] J.F. Ziegler, M.D. Ziegler and J.P. Biersack, SRIM: The stopping and range of ions in matter (2010), *Nuclear Instruments and Methods* **B268** (2010) 1818–1823. doi: 10.1016/j.nimb.2010.02.091
- [48] L.S. Waters, G.W. McKinney, J.W. Durkee, M.L. Fensin, J.S. Hendricks, M.R. James, R.C. Johns and D.B. Pelowitz, The MCNPX Monte Carlo radiation transport code, *AIP Conference Proceedings* **896** (2007) 81–90.
- [49] T. Mayer-Kuckuk, Kernphysik, Teubner, Stuttgart, 1984. ISBN 3-519-33021-0
- [50] W.N. McElroy, S. Berg, T. Crockett and R. G. Hawkins, A computer-automated iterative method for neutron flux spectra determination by foil activation - Vol. 1, AFWL-TR-67-41, Air Force Weapons Laboratory, 1967.
- [51] A.C. Fernandes, I. C. Gonçalves, J. Santos, J. Cardoso, L. Santos, A. Ferro Carvalho, J.G. Marques, A. Kling, A.J.G. Ramalho and M. Osvay, Dosimetry at the Portuguese Research Reactor using thermoluminescence measurements and Monte Carlo calculations, *Radiation Protection Dosimetry* **120** (2006) 349–353. doi:10.1093/rpd/nci560
- [52] A.C. Fernandes, J.P. Santos, J.G. Marques, A. Kling, A.R. Ramos and N.P. Barradas, Validation of the Monte Carlo model supporting core conversion of the Portuguese Research Reactor (RPI) for neutron fluence rate determinations, *Annals of Nuclear Energy* **37** (2010) 1139–1145. doi: 10.1016/j.anucene.2010.05.004
- [53] Y-F. Wang, V. Balic, G. Gratta, A. Fasso', S. Roesler and A. Ferrari, Predicting neutron production from cosmic-ray muons, *Physical Review* **D64** (2001) 013012-p.1–8. doi: 10.1103/PhysRevD.64.013012
- [54] D.M. Mei and A. Hime, Muon-induced background study for underground laboratories, *Physical Review* **D83** (2006) 053004-p.1–18. doi: 10.1103/PhysRevD.73.053004

- [55] T.A. Girard, A.R. Ramos, I.L. Roche and A.C. Fernandes, Phase III (and maybe IV) of the SIMPLE dark matter search experiment at the LSBB, *E3S Web of Conferences* **4** (2014) 01001-p.1–6. doi: 10.1051/e3sconf/20140401001